

# Correspondence

## Development of a Cybernetic Shoulder—A 3-DOF Mechanism That Imitates Biological Shoulder Motion

Masafumi Okada and Yoshihiko Nakamura

**Abstract**—In this paper, we develop a 3-degree of freedom (DOF) mechanism for humanoid robots, which we call the cybernetic shoulder. This mechanism imitates the motion of the human shoulder and does not have a fixed center of rotation, which enables unique human-like motion in contrast to the conventional design of anthropomorphic 7-DOF manipulators that have base three joint axes intersecting at a fixed point. Taking advantage of the cybernetic shoulder's closed kinematic chain, we can easily introduce the passive compliance adopting the elastic members. This is important for the integrated safety of humanoid robots that are inherently required to physically interact with the human.

**Index Terms**—Biological motion, closed kinematic chain, humanoid robot, passive compliance, shoulder mechanism.

### I. INTRODUCTION

As the research of humanoid robots goes on [1]–[4] and their application are discussed with reality, the importance of “mechanical softness” grows its importance. The mechanical softness ambiguously represents the hope that the physical presence of a humanoid robot among humans is naturally acceptable. The requirements for mechanical softness are wide, but would certainly include: 1) human-like high mobility and 2) human-like sensitive compliance. The present paper develops the idea of integration of mechanical softness, in particular, for humanoid shoulder.

**Human-like mobility** is demanded from the same reasons that demand the human-like geometry for a humanoid being in the human-structured environments. Furthermore, being among humans a humanoid is required to move with smooth and natural curves that we show using high degrees-of-freedom (DOF) mobility. It is important from the geometric functionality point of view and psychological one well. This requirement is contradict with one for mechanical simplicity from the implementation point of view and, therefore, poses an important design problem.

**Human-like sensitive compliance** is closely linked with the safety issue when a humanoid is among humans not only with the functionality in the human-structured environments. Contacts, collisions, and stability with their presence require a special attention for a humanoid robot. The technical discussions need to be elaborated on what kind of compliance to be integrated in a humanoid and how to implement it in the mechanism.

In this paper, we first see the mechanism of human shoulder and learn the nature of curves of shoulder motion. The cybernetic shoulder

Manuscript received January 8, 2002; revised June 1, 2002. This paper was recommended for publication by Associate Editor S. Ma and Editor F. Park upon evaluation of the reviewers' comments. This work was supported by the Research for the Future Program, the Japan Society for the Promotion of Science under Project JSPS-RFTF96P00801.

M. Okada is with the Department of Mechanical Sciences and Engineering, Tokyo Institute of Technology, Meguro-ku 152–8552, Japan (e-mail: okada@mep.titech.ac.jp).

Y. Nakamura is with the Department of Mechano-Informatics, University of Tokyo, Bunkyo-ku 113–8556, Japan (e-mail: nakamura@ynl.t.u-tokyo.ac.jp).

Digital Object Identifier 10.1109/TRO.2004.838006

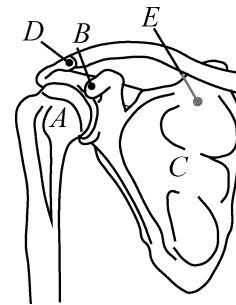


Fig. 1. Human shoulder mechanism.

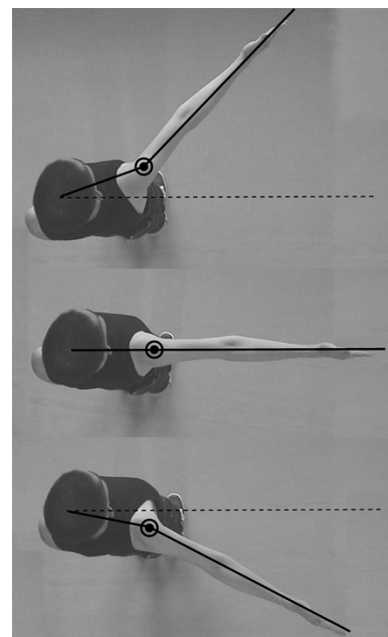


Fig. 2. Motion of the human shoulder.

is, then, proposed, designed and prototyped taking an advantage of parallel mechanism. Mathematics to solve the kinematics is also discussed and coded for real-time control. Section VI shows the human-like motion of the cybernetic shoulder comparing with the human motion and the humanoid shoulder motion with conventional design. Section VII describes our approaches and efforts to integrate mechanical compliance by adopting elastic and damping mechanical components as parts of the parallel mechanism. The experimental evaluation is also provided.

### II. HUMAN SHOULDER MECHANISM

Fig. 1 shows the human shoulder mechanism. The human shoulder is composed by five joints [5] that are split into two groups. One is a shoulder part (joint A and B), the other is a chest part (C, D, and E). These joints move dependently in each group so that the human shoulder can move smoothly [6]. Lenarčič analyzed the human shoulder complex comparing with the humanoid shoulder mechanism [7] from the mechanical point of view. Hannaford discussed the human shoulder mechanism from the actuator point of view [8]. Fig. 2

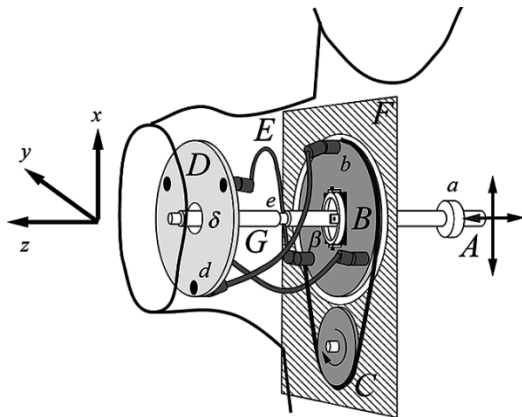


Fig. 3. Cybernetic shoulder.

shows the motion of the human shoulder. This figure shows that the human shoulder's motion does not have a fixed center of rotation [6], which causes the human-like motion. The conventional design of anthropomorphic 7-DOF manipulators do not realize this motion.

III. CONVENTIONAL MULTI-DOF MECHANISM

Position Controlling Apparatus has been developed by Pollard [9] in 1942. This is the first patented mechanism for wrist joints. Using a ball joint, links and tendons, the human's wrist motion is realized [3]. Because of the collision of a link and rod on roll motion, the workspace is not large.

PUMA robot has one of the most representative wrist joints. It is a roll-pitch-roll mechanism and the rotation axes of 3-DOF intersect at one point. Actuators are located in the lower arm.

Trevelyan has developed Elephant Trunk Wrist [10] for sheep shearing in 1985. This mechanism uses two sequential universal joints (double U-joint) coupled by a spur gear and imitates the elephant trunk motion.

Yoshikawa developed a 4-DOF wrist mechanism [11]. By the singularity avoidance using the redundant DOF and its control, the dynamic manipulability of the robot arm is improved. The rotation axes of 4-DOF cross at one point.

Rosheim enhanced the importance of the anthropomorphic mechanism for human-like smooth motion, and developed The Dexterous Arm [3] using a double U-Joint mechanism. The motions of two universal joints are coupled by a small gear and small volume is realized. The upper body humanoid robot has been developed [12] using the dexterous arm that has 5 DOF on the shoulder, 1 DOF on the elbow, and 3 DOF on the wrist. The DOF assignment is same as the human arm.

Stanišić has developed a symmetrically actuated system for a wrist joint using a semicircular link and spherical slider to avoid the singularity in the workspace [13]. And he has developed a robot arm [14] and a shoulder mechanism for humanoid robots [15].

IV. MECHANISM OF THE CYBERNETIC SHOULDER

Fig. 3 shows the model of the cybernetic shoulder, where  $\beta$  and  $\delta$  are 2-DOF gimbal mechanisms (universal joint),  $d$  is a 3-DOF ball joint,  $b$  is a 2-DOF universal joint,  $a$  is a 4-DOF joint of spherical and prismatic motion, and  $e$  is a prismatic joint. Moving the point  $A$  within the vertical plane alters the pointing direction of the main shaft  $G$ , which determines, along with the constraints due to the free curved links  $E$  between points  $b$  and  $d$ , the direction of the normal vector of  $D$ . The rotation about the normal of  $D$  is mainly determined by the rotation of  $C$  through  $B$  and  $G$ . Note that the rotation of  $C$  is coupled with the

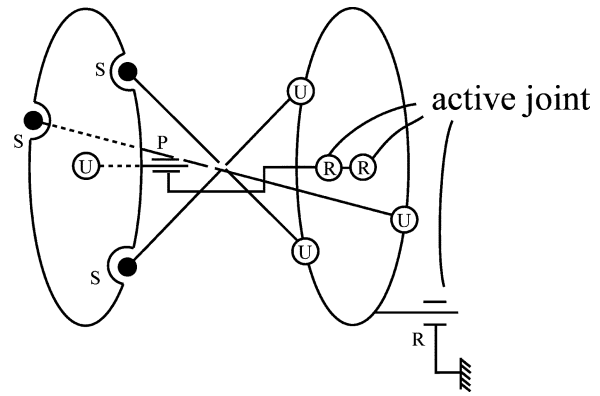


Fig. 4. Simplified model of the cybernetic shoulder.

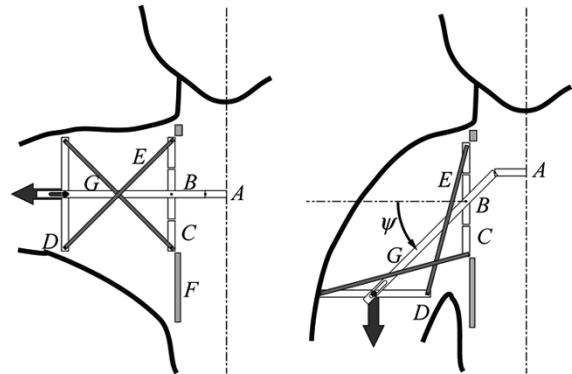


Fig. 5. Motion of the cybernetic shoulder.

pointing direction of  $D$  when  $B$  and  $D$  are not parallel. This mechanism is a 3SU-UPU mechanism. From Fig. 4, we obtain that the number of link is 8, the number of 3-DOF joint (spherical joint) is 3, the number of two DOF joints (universal joint) is 4 and the number of 1 DOF joints (rotational and prismatic joint) is 4, and the number of DOF of the cybernetic shoulder is calculated as

$$6 \times 8 - 3 \times 3 - 4 \times 4 - 5 \times 4 = 3. \tag{1}$$

The active joints are three rotational joints. Though two of active joints are activated by the motion of the point  $A$  in Fig. 3, it is equivalent to rotate two rotational joints for simplicity of the counting the number of DOF. The advantages of this mechanism are summarized as follows.

- a) *Compactness*: Since the cybernetic shoulder can locate its actuators inside the chest, the shoulder geometry occupies rather small volume and shows a smooth shape, compared with conventional designs of shoulder joints of manipulators.
- b) *Large workspace*: Fig. 5 shows the motion of the cybernetic shoulder, in the reduced two-dimensional model. When the main shaft  $G$  rotates  $\psi$  within  $\pm 45^\circ$ , the normal vector of  $D$  rotates within nearly twice as much as  $\pm 90^\circ$ . Although this magnification ratio is not constant, it generates a large workspace.
- c) *Human-like motion*: Fig. 6 shows a locus of center of rotation when point  $A$  moves along  $y$ -axis. This figure shows a distinctive characteristics that the center of rotation of the cybernetic shoulder makes a similar motion to that of the human shoulder motion as seen in Fig. 2. Note that the kinematics of the reduced two dimensional model of the cybernetic shoulder which is an anti-parallelogram mechanism [16] is different from that of three dimensional model, and it takes a different trajectory of the center of rotation that depends on the rotation of  $B$  in Fig. 3. The authors would like to claim that the cybernetic shoulder

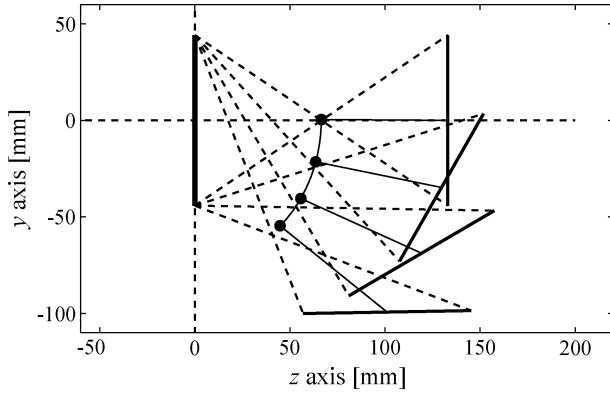


Fig. 6. Center of rotation.

generates with the reduced 3-DOF mechanism. The natural and smooth motions that the human shoulder does with higher DOF and higher mechanical complexity.

- d) *Singularity Free in Workspace*: As mentioned in the following, because the analytical solution of the forward and/or inverse kinematics of the cybernetic shoulder is difficult to obtain, the strict analysis of the singularity is difficult. However, it is true that in theoretically the range of the rotation of link  $G$  is  $|\psi| < 90^\circ$  because when  $|\psi| = 90^\circ$ , the point  $A$  is not defined, which means  $\psi = \pm 90^\circ$  implies singular points [17]. In practice, mechanical design limits the range of  $\psi$  a bit smaller. Although the upper limit of  $\psi$  depends on the rotation of plate  $B$  about  $z$ -axis, the range of  $\psi$  of the prototype spans  $\pm 45^\circ$  regardless of the rotation. This range of  $\psi$  enables the normal of plate  $D$  to span those of a hemisphere. This workspace is larger than that of the typical shoulders of conventional design. We make sure the singularity free in the workspace of the cybernetic shoulder by moving the prototype.
- e) *Small Backlash*: The cybernetic shoulder has a double universal-joint structure which yields a human shoulder geometry and has a human like motion. Many types of double universal-joint structures have already been reported [3], [9], [10] where the double universal-joint mechanisms were commonly driven by gears and, therefore, unfortunately suffer from large backlash. On the other hand, the constraints of the cybernetic shoulder are provided by closed kinematic chains and realize rather small backlash.

Figs. 7 and 8 show photographs of the prototyped cybernetic shoulder. The body height is about 400 mm, and the width between the end of the left and right shoulders is about 600 mm. The diameter of plate  $D$  is approximately 110 mm. The 3 DOF is directed by three 90-W DC motors. The planner motion of point  $A$  is made by two perpendicular ball-screw axes assembled in series.

## V. KINEMATICS OF THE CYBERNETIC SHOULDER

Due to the complexity of a closed kinematic chain of the cybernetic shoulder, it is difficult to obtain the analytical solution of inverse or forward kinematics. We, therefore, apply a numerical method to solve the kinematics. Because the cybernetic shoulder has 3 DOF, we give the orientation of the end plate  $D$  and obtain the rotation angle of the three active joints, which is inverse kinematics.

We define parameters and coordinate systems as shown in Fig. 9.  $x_0y_0z_0$  is the absolute coordinate system with the origin at  $\beta$ , center of  $B$ .  $x_e y_e z_e (= x_5 y_5 z_5)$  is the end plate coordinate system with the origin at  $\delta$ , center of  $D$ . The rotation of plate  $B$  is measured from

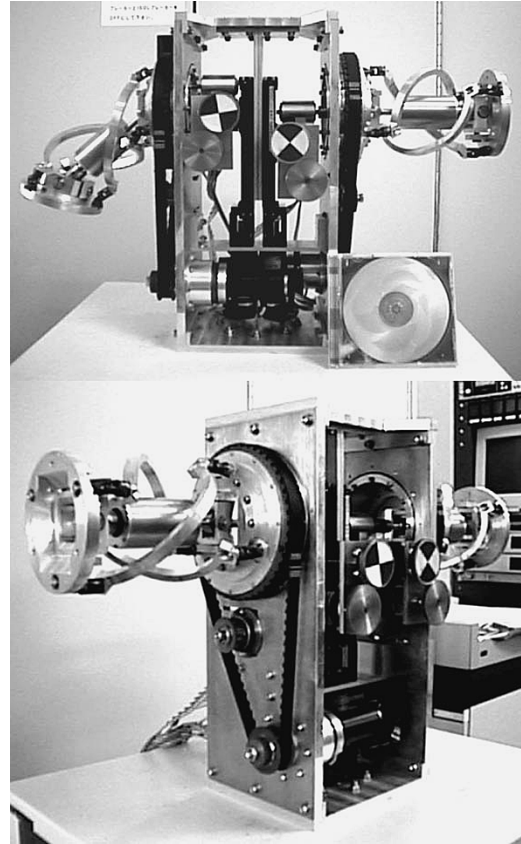


Fig. 7. Photographs of the cybernetic shoulder.

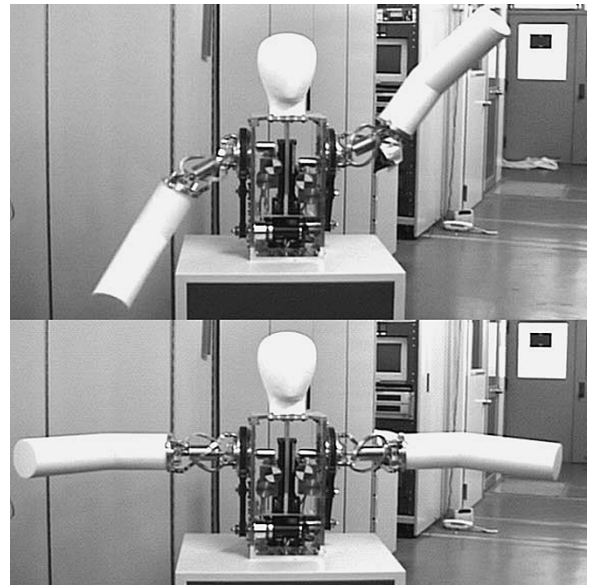


Fig. 8. Motion of the experimental system.

$x_0$ -axis and takes zero degree when  $\mathbf{b}_1$  has the same direction as  $x_0$ . In Fig. 9, plate  $B$  is rotated  $\phi$  about  $z_0$ -axis. In the following,  $[\cdot]^i$  means a vector in  $x_i y_i z_i$  coordinate system and  $\mathbf{R}_\theta^\xi$  implies the rotation of  $\theta$  about  $\xi$ -axis. Accordingly

$$\mathbf{b}_i^0 = \mathbf{R}_\phi^{z_0} \mathbf{R}_\theta^{z_0} \mathbf{R}_{\frac{2}{3}(i-1)\pi} [r \ 0 \ 0]^T \quad (2)$$

$$\mathbf{d}_i^e = \mathbf{R}_{\frac{2}{3}(i-1)\pi}^{z_0} [r \ 0 \ 0]^T \quad (3)$$

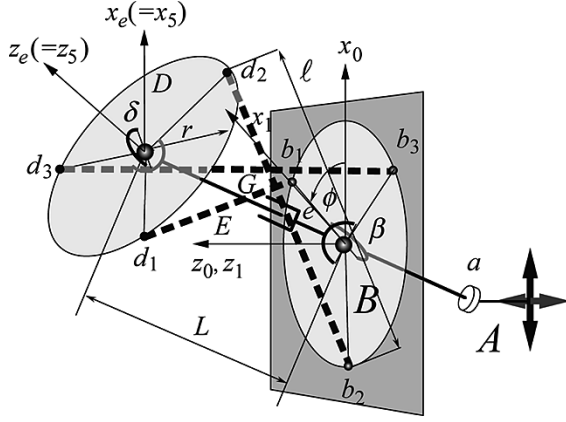


Fig. 9. Model of the cybernetic shoulder.

are satisfied. Since  $\beta$  and  $\delta$  have gimbal mechanisms, we consider  $\theta_{x1}$  as the rotation about  $x_1$ -axis,  $\theta_{y2}$  as the rotation about  $y_2$ -axis,  $\theta_{y3}$  as the rotation about  $y_3$ -axis and  $\theta_{x4}$  as the rotation about  $x_4$ -axis in order like an euler angle coordinates. We then obtain the following equations:

$$\mathbf{d}_i^0 = \delta + \mathbf{R}\mathbf{d}_i^e \quad (i = 1, 2, 3) \quad (4)$$

$$\delta = L\mathbf{R}_A\mathbf{e}_z \quad (5)$$

$$\mathbf{R} = \mathbf{R}_A\mathbf{R}_B \quad (6)$$

$$\mathbf{R}_A = \mathbf{R}_{\theta_{x1}}^{x1} \mathbf{R}_{\theta_{y2}}^{y2} \quad (7)$$

$$\mathbf{R}_B = \mathbf{R}_{\theta_{y3}}^{y3} \mathbf{R}_{\theta_{x4}}^{x4} \mathbf{R}_{\pi}^{z5} \quad (8)$$

$$\mathbf{e}_z = [0 \ 0 \ 1]^T \quad (9)$$

where  $\theta_{x1}$  and  $\theta_{y2}$  are determined by the position of  $A$  and  $\phi$  is determined by the rotation angle of  $B$ . Variables such as  $\theta_{y3}$ ,  $\theta_{x4}$  and  $L$  are to be computed. From the kinematic constraints of that the lengths of link  $E$  are constant, we have

$$|\mathbf{d}_i^0 - \mathbf{b}_i^0| = \ell_i \quad (10)$$

where we set  $\ell_1 = \ell_2 = \ell_3 = \ell$ . From (4), the above equation is written as follows:

$$|\mathbf{L}\mathbf{R}_A\mathbf{e}_z + \mathbf{R}\mathbf{d}_i^e - \mathbf{b}_i^0| = \ell_i \quad (11)$$

To solve this equation, we apply gradient based numerical computation. We set the cost function  $J$  as follows:

$$J = \sum_{i=1}^3 J_i^2 \quad (12)$$

$$J_i = |\mathbf{L}\mathbf{R}_A\mathbf{e}_z + \mathbf{R}\mathbf{d}_i^e - \mathbf{b}_i^0| - \ell_i \quad (i = 1, 2, 3). \quad (13)$$

Defining  $T_{\theta_{x4}}$  and  $T_{\theta_{y3}}$  as

$$T_{\theta_{x4}} = \tan \frac{\theta_{x4}}{2} \quad (14)$$

$$T_{\theta_{y3}} = \tan \frac{\theta_{y3}}{2} \quad (15)$$

we calculate

$$T_{\theta_{x4}} = T_{\theta_{x4}} - k_1 \frac{\partial J}{\partial T_{\theta_{x4}}} \quad (16)$$

$$T_{\theta_{y3}} = T_{\theta_{y3}} - k_2 \frac{\partial J}{\partial T_{\theta_{y3}}} \quad (17)$$

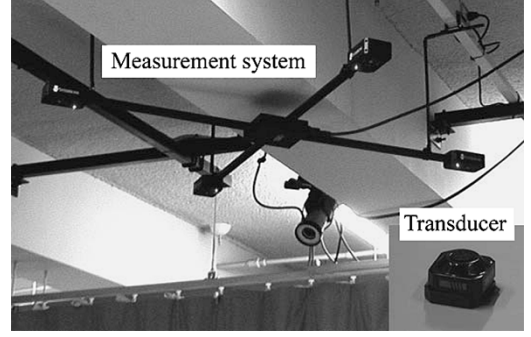


Fig. 10. Motion measurement system.

$$L = L - k_3 \frac{\partial J}{\partial L} \quad (18)$$

iteratively, where  $k_1$ ,  $k_2$ ,  $k_3$  are constant and  $\partial J/\partial T_{\theta_{x4}}$ ,  $\partial J/\partial T_{\theta_{y3}}$ ,  $\partial J/\partial L$  are given by

$$\frac{\partial J}{\partial s} = 2 \sum_{i=1}^3 \frac{\partial J_i}{\partial s} J_i \quad (s = T_{\theta_{x4}}, T_{\theta_{y3}}, L) \quad (19)$$

$$\frac{\partial J_i}{\partial L} = |\mathbf{R}_A\mathbf{e}_z| \quad (20)$$

$$\frac{\partial J_i}{\partial T_{\theta_{x4}}} = \left| L \frac{\partial \mathbf{R}_A}{\partial T_{\theta_{x4}}} \mathbf{e}_z + \frac{\partial \mathbf{R}}{\partial T_{\theta_{x1}}} \mathbf{d}_i^e \right| \quad (21)$$

$$\frac{\partial J_i}{\partial T_{\theta_{y3}}} = \left| L \frac{\partial \mathbf{R}_A}{\partial T_{\theta_{y3}}} \mathbf{e}_z + \frac{\partial \mathbf{R}}{\partial T_{\theta_{y3}}} \mathbf{d}_i^e \right| \quad (22)$$

using  $\theta_{x1}$ ,  $\theta_{y2}$  and current values of  $\theta_{x4}$ ,  $\theta_{y3}$  and  $L$ . We verified that the cost function  $J$  converged to zero with the accuracy of  $\pm 2\%$  for small movements of the orientation of the end plate within ten times iterations. By using reference of the motor rotation angles obtained by the above computation, each motor is controlled by PD controller.

## VI. COMPARISON WITH THE HUMAN MOTION

### A. Measurement

We show the human-like motion of the cybernetic shoulder by comparing with the natural human motion. The human shoulder has 5 DOF, it is able of the variety of motions. However the cybernetic shoulder has 3 DOF and cannot realize the exactly same motions as a human shoulder. Lenarčič discussed the human likeness from the mechanical point of view [7]. In this paper, we focus on the human daily motion that is, for example, drinking a cup of coffee. Obtaining the motion data from the motion measurement system, we discuss the human likeness of the cybernetic shoulder. Fig. 10 shows the motion measurement system. This system measures 3-D positions of the transducers using ultrasonic sound. We use 6 transducers allocated as shown in Fig. 11, and measure the human motion of drinking a cup of coffee. Transducer 1 (T1) is on the head, T2 is on the table that defines the absolute coordinate system, T3 is on the base of the neck, T4 is on the shoulder, and T5 and T6 are at the elbow and wrist joint respectively. Fig. 12 shows the measured motion. Starting from the initial position, the subject takes a cup, drinks coffee and puts it back.

Fig. 13 shows the trajectory of the shoulder (T4) about  $y$ -axis. In the catching and releasing motion, the subject moves his arm and shoulder to reach the cup.

### B. Evaluation

For the evaluation of the human-likeness of the cybernetic shoulder, we set the following method.

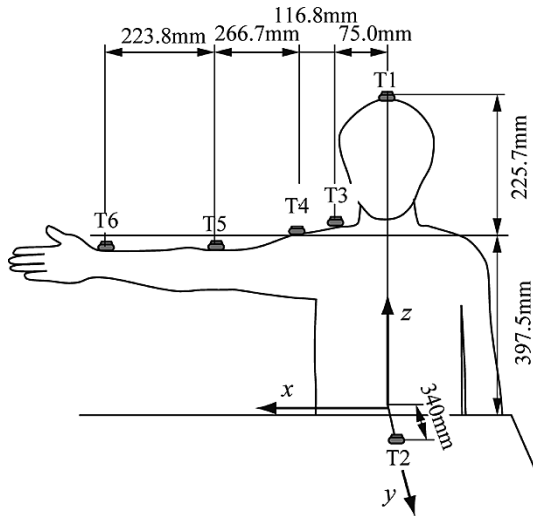


Fig. 11. Position of transducers.

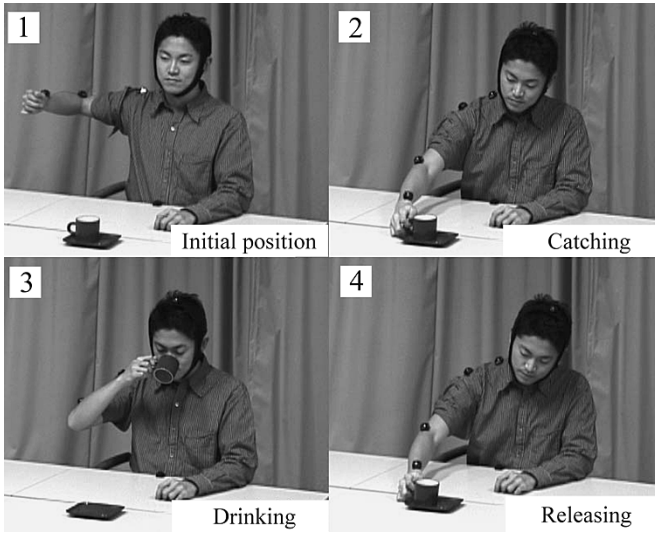


Fig. 12. Measured motion.

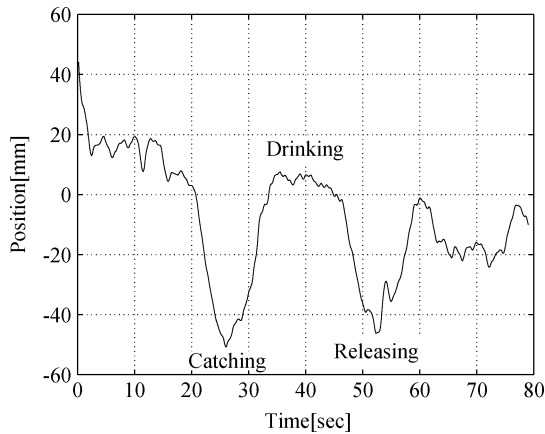


Fig. 13. Locus of the shoulder.

**Evaluation method:** We set a humanoid robot that has the same size as the subject, and set representative points  $x_i(t)$  ( $i = 1, 2, \dots, 6$ ) whose positions are equivalent to the positions of the transducers

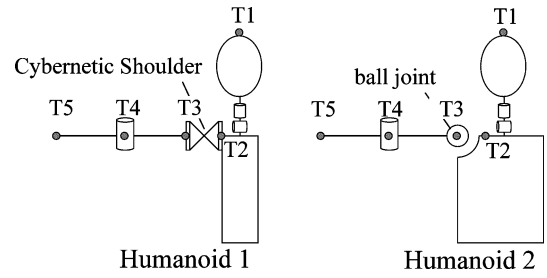


Fig. 14. Two humanoid robots for the evaluation.

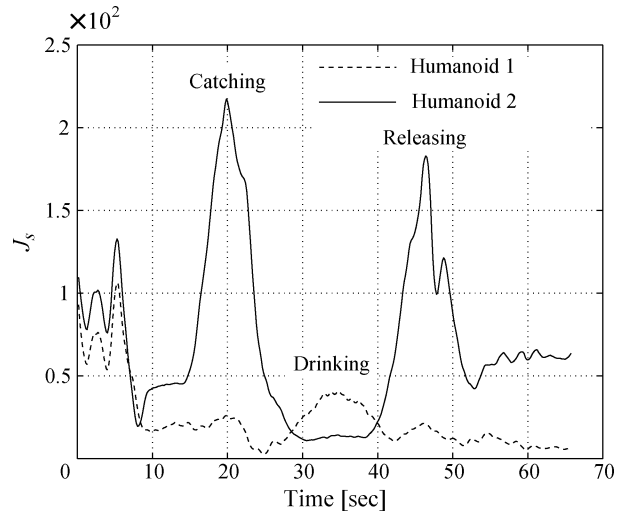


Fig. 15. Value of  $J_s(t)$ .

$X_i(t)$  ( $i = 1, 2, \dots, 6$ ) on the subject. Setting the cost function  $J_s(t)$  as follows:

$$J_s(t) = \sum_{i=1}^6 \sqrt{\Delta x_i^T(t) \Delta x_i(t)} \quad (23)$$

$$\Delta x_i(t) = X_i(t) - x_i(t) \quad (24)$$

we obtain  $x_i(t)$  ( $i = 1, 2, \dots, 6$ ) that minimizes  $J_s(t)$  in each time and we calculate  $J$

$$J = \int_0^T J_s(t) dt \quad (25)$$

that is the human-likeness index of the humanoid motion, where  $T$  is the measuring time.

We set two humanoid robots as shown in Fig. 14. One has the cybernetic shoulder (Humanoid 1), another has a conventional design of the shoulder mechanism with the fixed center of rotation (Humanoid 2), and we obtain the motions that minimize (23). The values of  $J$  for Humanoid 1 ( $J^1$ ) and Humanoid 2 ( $J^2$ ) are obtained as follows:

$$J^1 = 1.56 \times 10^5 \quad (26)$$

$$J^2 = 4.70 \times 10^5 \quad (27)$$

Fig. 15 shows the value of  $J_s(t)$  according to the time. The difference between two humanoid robots is remarkable in catching and releasing motion. Fig. 16 shows the postures of the humanoid robots at catching point (20 s). The dashed line with mark “\*” shows the posture of the subject and the solid lines with mark “o” show the postures of humanoid robots. The work space of Humanoid 1 is larger than that of Humanoid 2 because of the motion of the shoulder. These results show

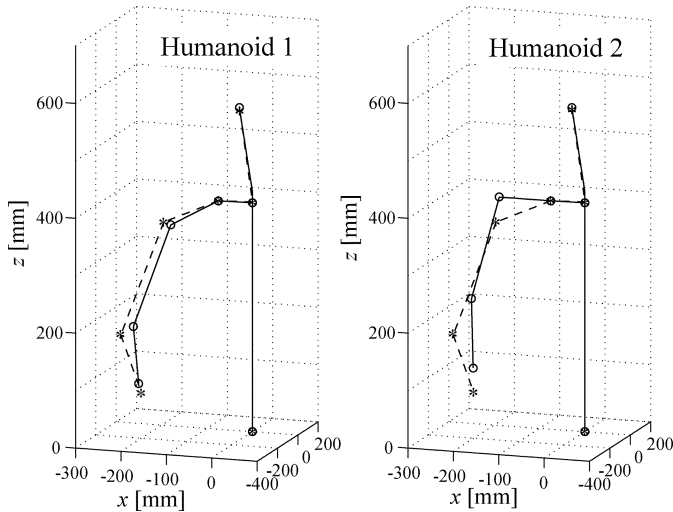


Fig. 16. Position of torsos.

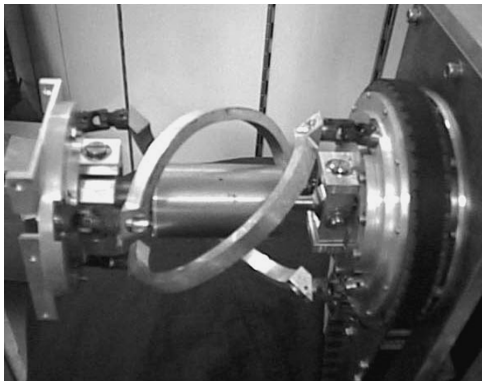


Fig. 17. Cybernetic shoulder with rigid link.

that the humanoid robot with the cybernetic shoulder has as large as human shoulder workspace same as other double U-joint mechanisms [3]. In addition to that, the cybernetic shoulder has a small backlash and compact volume because of the closed kinematic chain. From these results, the cybernetic shoulder is suitable for the compact humanoid robot from the mechanical design point of view.

VII. PASSIVE COMPLIANCE

A humanoid robot requires mechanical softness so as not to injure the humans sharing the common space. Using the closed kinematic chain of the cybernetic shoulder, we can easily integrate the softness of mechanism. The compliance of the cybernetic shoulder can be realized by properly designing parameters of link *E* in Fig. 3. We would like to show a few examples of such implementations.

Fig. 17 shows the link *E* using the original rigid material of aluminum alloy (Type 1). As an attempt to implement passive compliance, a thin carbon fiber ( $\phi 3$  mm) rod is used as an elastic material in Fig. 18 (Type 2). The shape of this link is shown in Fig. 19. As shown later, this link had large compliance and small damping. Fig. 20 shows the  $\phi 5$ -mm carbon fiber link with a damper (Type 3). The damper is designed as shown in Fig. 21 using Temper Foam.<sup>1</sup> The spring constant and the coefficient of viscosity of the three type of links are shown in Table I. By using carbon rods, mechanical softness is realized. The

<sup>1</sup>Temper Foam: Produced by EAR SPECIALITY COMPOSITES Corporation. shows frequency dependent characteristics. Namely, it shows high stiffness for high frequency and high viscosity for low frequency.

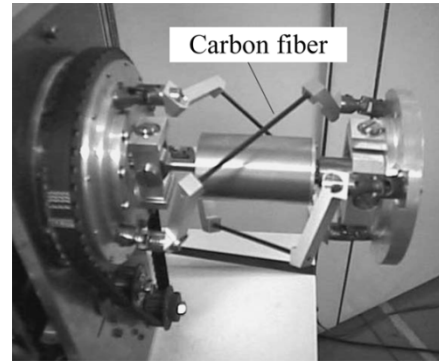


Fig. 18. Cybernetic shoulder with carbon fiber link.

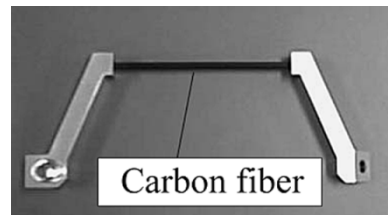


Fig. 19. Prototype of the link *E*.

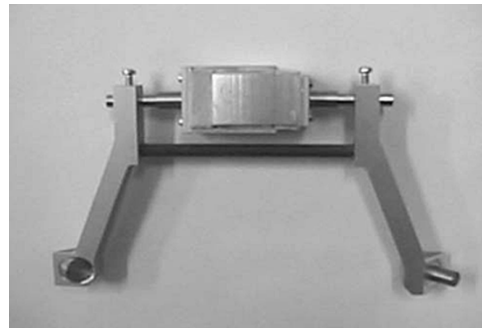


Fig. 20. Link *E* with a damper.

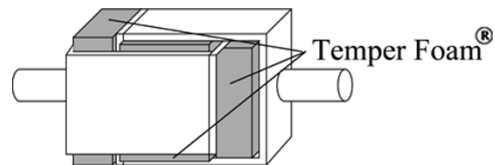


Fig. 21. Design of a damper.

TABLE I  
SPRING CONSTANT AND COEFFICIENT OF VISCOSITY

Type	Spring Constant (N/m)	Coefficient of viscosity (kg/s)
1	$1.609 \times 10^3$	0.625
2	$1.485 \times 10^2$	0.660
3	$5.963 \times 10^2$	1.05

impulse responses of the end plate of the cybernetic shoulder using  $\phi 3$ -mm carbon link (Type 2) and the  $\phi 5$ -mm carbon link with damper (Type 3) are shown in Fig. 22, where magnitudes of the initial conditions are normalized. The designed damper has large effectiveness for the viscosity of the cybernetic shoulder.

For the precision and ease of control, high stiffness is suitable, while the safety consideration requires low stiffness. To technically compromise these two conflicting requirements, two approaches are helpful.

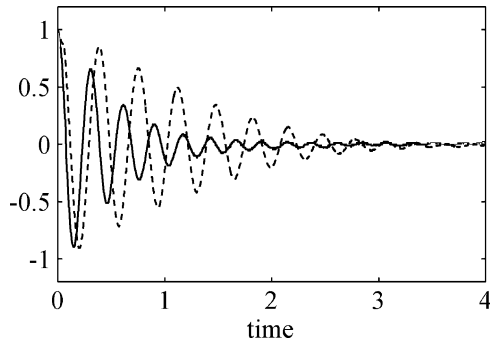


Fig. 22. Impulse responses (dashed line: type 2; solid line: type 3).

One is the use of a nonlinear elastic link. An example of such elasticity is one known for the TiNi shape memory alloy (SMA). When the strain is large, the maximum stress is limited. It is also known that elasticity and viscosity can be controlled by changing temperature of SMA. Adopting SMA as link material can be a promising approach to integrate a safety of the humanoid robot. The other is a joint design of active and passive compliance. By coupling these two compliances, we will obtain the appropriate compliance characteristic, which will be one of our future problems.

#### VIII. CONCLUSION

In this paper, we have proposed, designed and fabricated the new mechanism cybernetic shoulder for the humanoid robot shoulder.

- 1) The advantages of the cybernetic shoulder are compactness, large workspace, human-like motion, singularity free in the workspace and small backlash. And because of the closed kinematic chain, it is easy to introduce the mechanical compliance to the cybernetic shoulder.
- 2) We have discussed mathematics to solve the kinematics of the cybernetic shoulder.
- 3) We evaluate the human-like motion of the cybernetic shoulder by comparing with the human natural motion.
- 4) We can design the elasticity and the viscosity of the cybernetic shoulder by changing the material of link  $E$  which determines the kinematic constraints.
- 5) We have designed two types of new link  $E$ . One is  $\phi 3$  mm carbon fiber link which has large compliance and small damping. The other is a  $\phi 5$ -mm carbon fiber link with a damper using Temper Foam.

#### REFERENCES

- [1] J. Yamaguchi and A. Takanishi, "Development of a biped walking robot having antagonistic driven joints using nonlinear spring mechanism," in *Proc. IEEE Int. Conf. Robotic Automation*, 1997, pp. 185–192.
- [2] K. Hirai *et al.*, "The development of Honda humanoid robot," in *Proc. IEEE Int. Conf. Robotic Automation*, 1997, pp. 1321–1326.
- [3] M. E. Rosheim, *Robot Evolution, The Development of Anthropotics*. New York: Wiley, 1994.
- [4] M. Inaba *et al.*, "A remote-brain full-body humanoid with multisensor imaging system of binocular viewer, ears, wrist force and tactile sensor suit," in *Proc. Int. Conf. Robotic Automation*, 1997, pp. 2497–2502.
- [5] A. E. Emgin and S. T. Tümer, "Three-dimensional kinematic modeling of the human shoulder complex—part I: physical model and determination of joint sinus cones," *ASME J. Biomech. Eng.*, vol. 111, pp. 107–121, 1989.
- [6] I. A. Kapandji, *Physiologie Articulare*, France: Maloine, 1980.
- [7] J. Lenarčič and M. Stanišić, "A humanoid shoulder complex and the humanoid pointing kinematics," *IEEE Trans. Robot. Autom.*, vol. 19, no. 3, pp. 499–506, Jun. 2003.

- [8] B. Hannaford, J. M. Winters, C. C. Chou, and P. H. Marbot, "The anthropomorphic biorobotic arm: a system for the study of spinal circuits," *Ann. Biomed. Eng.*, vol. 23, pp. 399–408, 1995.
- [9] W. Pollard, "Position controlling apparatus," U.S. Patent 2 286 571, Jun. 16, 1942.
- [10] J. P. Trevelyan, "Skills for a shearing robot: dexterity and sensing," *Robot. Res.*, pp. 273–280, 1985.
- [11] T. Yoshikawa and S. Kiriya, "Four-joint redundant wrist mechanism and its control," *Trans. ASME J. Dyn. Syst. Meas. Control*, vol. 111, pp. 200–204, Jun. 1989.
- [12] M. Rosheim, "In the footsteps of Leonardo," *IEEE Robot. Autom. Mag.*, vol. 4, no. 2, pp. 12–14, Jun. 1997.
- [13] M. M. Stanišić and O. Duta, "Symmetrically actuated double pointing system: the basis of singularity-free robot wrists," *IEEE Trans. Robot. Autom.*, vol. 6, no. 5, pp. 562–569, Oct. 1990.
- [14] S. J. Remis and M. M. Stanišić, "Design of a singularity-free articulated arm subassembly," *IEEE Trans. Robot. Autom.*, vol. 9, no. 6, pp. 816–824, Dec. 1993.
- [15] M. M. Stanišić *et al.*, "A dexterous humanoid shoulder mechanism," *J. Robot. Syst.*, vol. 18, no. 12, pp. 737–745, 2001.
- [16] R. Beyer, "Kinematische Getriebelehre," in *Grundlagen einer quantitativen Getriebelehre ebener Getriebe, für den Konstrukteur, die Vorlesung und das Selbststudium*. Berlin, Germany: Springer-Verlag, 1953.
- [17] R. L. Willams, "Singularities of a manipulator with offset wrist," *ASME J. Mech. Des.*, vol. 121, no. 2, pp. 315–319, 1999.